An estimate of the macroscopic yield surfaces of powder compacts using the kinematic approach of the yield design theory

Anouar BENABBES[1], Luc DORMIEUX[2] and Larbi SIAD[1]

[1] *GMMS, URCA - Moulin de la Housse, BP 1039, 51687 Reims Cedex 2, France.*
E-mail : anouar.benabbes@univ-reims.fr ; larbi.siad@univ-reims.fr
[2] *LMSGC, ENPC, 6 et 8 avenue Blaise Pascal, Cité Descartes, Champs-sur-Marne, 7455 Marne la Vallée cedex 2, France.*
E-mail : Dormieux@lmsgc.enpc.fr

Abstract- The $3D$ compaction of a square array of spherical particles of uniform size is studied using the kinematic approach of the yield design theory. The densification is assumed to occur by plastic deformation at the mutual zone contacts between grains where the dissipation is localized. The compaction response of the array of spherical particles is considered in term of representative unit cell of the aggregate submitted to axisymmetrical loading conditions. Approximate macroscopic yield surfaces resulting from hydrostatic and closed die compaction are constructed at various stages of densifications. The size and shape of the yield surfaces depend upon the loading history as well as the relative density of the compact. Finite element simulations have also been performed in order to validate to some extent the results provided by the kinematic approach of the yield design theory and to examine the evolution of macroscopic yield surface with the degree of compaction.

Keywords- Powder compaction. Finite element. Kinematic approach. Macroscopic yield surface. Relative density. Spherical particles. Unit cell. Yield design theory.

1 INTRODUCTION

Among the industrial manufacturing processes used to obtain components of rather complicated geometry the powder compaction is more and more requested. The powder metallurgy industry is based upon the process of cold compaction of powder followed by sintering. Here only the compaction is considered. Cold compaction occurs within a closed die or in a cold isostatic press. Three different stages of powder compaction may be identified as follows. "Stage 0" is the initial rearrangement of powder particles. The second stage compaction, "stage I", corresponds to the situation for which contact size between individual particles increases but the relative density is low (ranging from the random close package value of 0.64 up to around 0.9). The final stage compaction, "stage II", starts when plastic flow spreads throughout each particle and only small holes between particles remain (refer to review article [5]).

Akisanya *et al.* [4] have used slip-line field and finite element methods to study the evolution, under hydrostatic and closed die compaction, of macroscopic yield surfaces for stage I compaction of an hexagonal array of uniform circular cylinders. More recently Sridhar *et al.* [1] have studied the biaxial compaction of a square array of uniform circular cylinders using slip-line field, upper bound (kinematic approach) and finite element methods to examine, under hydrostatic and closed die compaction, the evolution of contact size, contact pressure and macroscopic yield surfaces for stage I and II of compaction. Ogbonna and Fleck [3] have studied the three-dimensional compaction response of an array of identical spherical particles in terms of a representative unit cell of the aggregate submitted to axisymmetrical loading conditions. They used only numerical simulations investigation to examine the evolution of contact size, contact pressure and macroscopic yield surfaces for stage I and II of compaction. In this study the focus of the analysis in on powder compaction and the kinematic approach of the yield design theory [2] is used as the technique of solution for the construction of an estimate of the macroscopic yield surfaces of the powder compacts. The obtained results are compared to numerical ones issued from the compaction response of a representative unit cell as adopted by Ogbonna and Fleck [3].

2 POWDER STRUCTURE AND UNIT CELL

The arrangement of powder for this study consists of a simple cubic array of homogeneous spherical particles of uniform size *Fig.1(a)*. The cubic array of spheres is submitted to axisymmetrical loading conditions. The deformation of powder aggregates is essentially controlled by contacts between spheres, with the spheres initially touching each other at six contact points. The compaction response of the cubic array of spherical particles is considered in terms of a representative unit cell of the aggregate. Following Ogbana and Fleck [3], the unit cell is taken to be a single spherical particle circumscribed by a circular cylinder the height of which is twice the radius of the undeformed sphere R_o, *Fig.1(b)*. In fact, during compaction, the top and bottom planes of the unit cell surrounding a representative particle approach each other, and the cylindrical boundary of the cell shrinks in diameter that can be interpreted as the contribution from the four particle contacts surrounding the mid-section of a typical particle. The deformed state of the unit cell is illustrated in *Fig.2*, showing characteristic dimensions and macroscopic stresses.

The relative density D is defined here as the ratio of the average density of the powder to that of the fully dense solid. By conservation of mass an expression of D is

$$D = \frac{2}{3}\frac{R_o^3}{R^2 H} \tag{1}$$

Its initial value is $2/3$ that is very close to 0.64 for a random close package of equi-sized spherical particles.

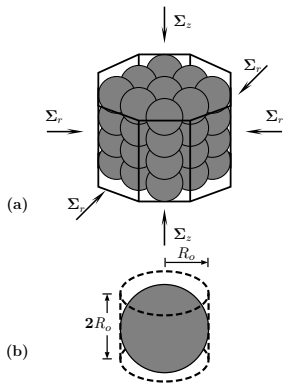

FIG. 1 – (a) Simple cubic array arrangement of powder. (b) Representative unit cell.

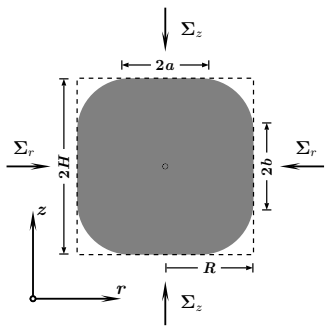

FIG. 2 – Deformed state of the unit cell showing characteristic dimensions and axisymmetric macroscopic stresses.

The macroscopic response of the aggregate is given by the average state of strain and stress in the representative unit cell. The logarithmic radial E_r and axial E_z strains are given by

$$E_r = \ln\left(\frac{R}{R_o}\right) \ , \ E_z = \ln\left(\frac{H}{R_o}\right) \tag{2}$$

resulting in

$$D = D_o \, \exp\{-(2E_r + E_z)\} \tag{3}$$

Σ_m and Σ denote the macroscopic mean and deviatoric stresses which expressions are

$$\Sigma_m = (2\Sigma_r + \Sigma_z)/3 \ , \ \Sigma = \Sigma_z - \Sigma_r \tag{4}$$

3 THE KINEMATIC APPROACH

The objective of kinematic approach of the yield design theory is to provide an estimate of stability conditions for a mechanical system irrespective of the behaviour of the constituent materials [2]. Stability conditions are expressed in terms of the intensity of loads that can be applied to the system without implying its collapse. An upper bound estimate of such loads is found by considering kinematically admissible failure mechanism for which the work done by the loads applied to the system is larger than the maximum resisting work that can be mobilized inside the system. In addition, any set of loads for which a stress field can be found that satisfies equilibrium and the material yield criterion, is a lower bound solution.

The upper bound method assume a rigid, ideally plastic material response. In order to specify the evolution of contact size between particles, as a function of macroscopic strain, a number of additional geometrical assumptions are required : In stage I, the free surface of the particle has a uniform radius $\tilde{R} > R_o$ and in stage II, the pore is treated as quadratic in shape with side length s.

When the kinematic approach is applied to rigid, ideally plastic solids, the deformation state consists of regions, sliding relative to each other. The velocity field mobilized in each region can be taken as $\underline{V} = V_r \underline{e}_r + V_z \underline{e}_z$ with respect to cylindrical coordinates system (r, z), and should be verify the incompressibility behaviour of the solid, i.e., $\mathrm{div}\,\underline{V} = 0$. In cylindrical coordinates system this constraint results in $V_r = A/r$ and $V_z = w$, where A and w are a constants.

Fig.3 shows some of the possible upper bound mechanisms that can exist within the unit cell of the spherical array during the stage I densification. Mechanisms $\mathbb{A}$ and $\mathbb{B}$ are simple indentation fields at each contact and are relevant when the contacts are small. The collapse mechanisms $\mathbb{A}$ and $\mathbb{B}$ have two degrees of freedom specified by χ and ρ. Typical velocity fields are included in the figures. The macroscopic yield surface is obtained by making the rate of external work is larger than the rate of internal plastic work dissipation, given by equations

$$2\pi R^2 w_1 \Sigma_z \ \leq \ \mathcal{P}_{mr}, \tag{5}$$

$$4\pi H A \Sigma_r \ \leq \ \mathcal{P}_{mr}, \tag{6}$$

for the collapse mechanisms $\mathbb{A}$ and $\mathbb{B}$, respectively. The right-hand side $\mathcal{P}_{mr}$ is defined by

$$\mathcal{P}_{mr} = \int_\Omega \Pi(\underline{\underline{d}}) dV + \int_S \Pi(\underline{n}, [\![\underline{V}]\!]) d\Sigma, \tag{7}$$

where $\Pi(\underline{\underline{d}})$ and $\Pi(\underline{n}, [\![\underline{V}]\!])$ is giving, for a von-Mises material, by

$$\begin{cases} \Pi(\underline{\underline{d}}) = +\infty, & \text{if } \mathrm{tr}\underline{\underline{d}} \neq 0\,; \\ \Pi(\underline{\underline{d}}) = \sigma_y/\sqrt{3}\,\sqrt{2\mathrm{tr}(\underline{\underline{d}})^2}, & \text{if } \mathrm{tr}\underline{\underline{d}} = 0. \end{cases} \tag{8}$$

$$\begin{cases} \Pi(\underline{n}, [\![\underline{V}]\!]) = +\infty, & \text{if } [\![\underline{V}]\!].\underline{n} \neq 0\,; \\ \Pi(\underline{n}, [\![\underline{V}]\!]) = \sigma_y/\sqrt{3}\,|[\![\underline{V}]\!]|, & \text{if } [\![\underline{V}]\!].\underline{n} = 0. \end{cases} \tag{9}$$

where σ_y is the uniaxial yield stress of the particles material. For a given values of a, b, H and R, the best estimate of Σ_z or Σ_r is the optimum value obtained by varying χ and ρ in the equations (5) and (6). In mechanisms $\mathbb{D}$ and $\mathbb{E}$ there is an interaction between the deformation of contacts and there is also a contact which is loaded more than the other contact. The collapse mechanisms $\mathbb{D}$ and $\mathbb{E}$ have two degrees of freedom χ and ψ, as shown. For an assumed value of Σ_r, the best estimate of Σ_z is the minimum value obtained by varying χ and ψ in the equations

$$2\pi R^2 w_1 \Sigma_z + 4\pi H A \Sigma_r \ \leq \ \mathcal{P}_{mr}, \tag{10}$$

$$2\pi R^2 w_2 \Sigma_z + 4\pi H A \Sigma_r \ \leq \ \mathcal{P}_{mr}, \tag{11}$$

for the collapse mechanisms $\mathbb{D}$ and $\mathbb{E}$, respectively.

Fig.4 shows some of the possible upper bound mechanisms that can exist within the unit cell of the spherical array during the stage II densification. Mechanisms $\mathbb{I}$ and $\mathbb{J}$ are produced when the plastic zone under a contact interacts with the free surface of the adjacent pore. The collapse mechanisms $\mathbb{I}$ and $\mathbb{J}$ have two degrees of freedom ρ and l. For a given values of a, b, H and R, the best estimate of Σ_z or Σ_r is the optimum value obtained by varying χ and ρ in the equations (5) and (6) for the collapse mechanisms $\mathbb{I}$ and $\mathbb{J}$, respectively. The mechanisms $\mathbb{H}$ and $\mathbb{G}$ are obtained when opposing contacts are loaded more heavily than the neighbouring contacts and the material is extruded side-ways. Unlike previous mechanisms, the mechanisms $\mathbb{H}$ and $\mathbb{G}$ have no degrees of freedom. For an assumed value of Σ_r, the best estimate of Σ_z is obtained by the equations (10) and (11) for the collapse mechanisms $\mathbb{H}$ and $\mathbb{G}$, respectively.

The macroscopic yield surfaces obtained from previous mechanisms by mean of the kinematic approach, for both

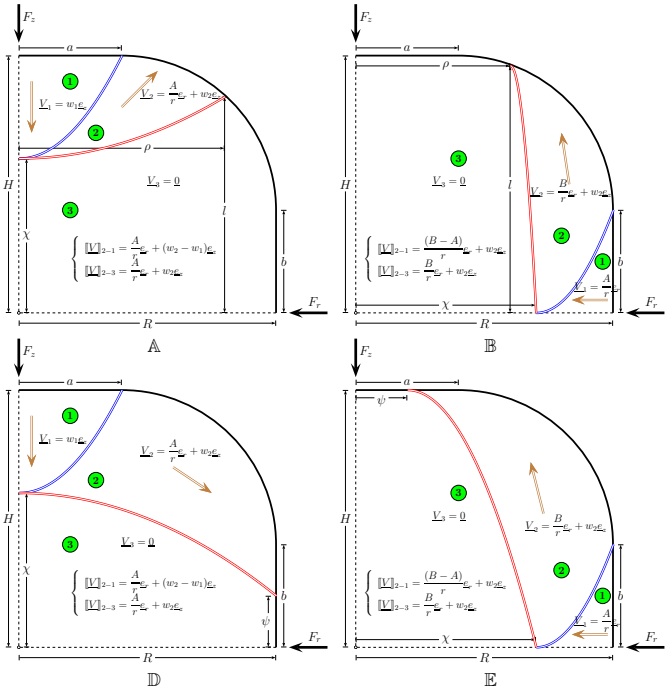

FIG. 3 – Four proposed upper bound collapse mechanisms for stage I compaction.

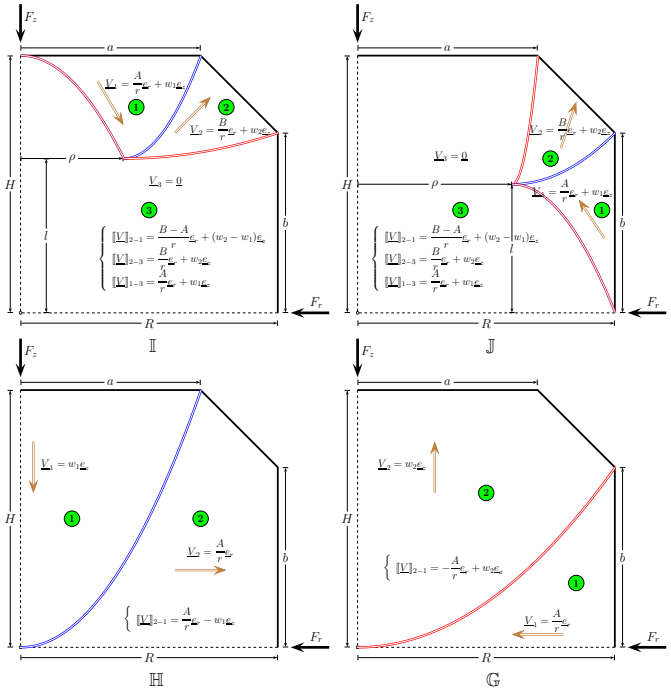

FIG. 4 – Four proposed upper bound collapse mechanisms for stage II compaction.

stages I and II, are plotted in *Fig.5* for hydrostatic compaction and in *Fig.6* for closed die compaction. For both figures, macroscopic yield surfaces are shown in (Σ_r, Σ_z) space and in (Σ_m, Σ) space, and are compared with the numerical results provides by the finite element analysis. The straight line segments obtained from the kinematic approach refer to the activated mechanism of deformation. For clarity of the plots, we have not mention the referred letter's mechanism to each straight line segments. The results obtained by the kinematic approach is adequate with the finite element predictions that is taken as the reference solutions for the yield surfaces. Differences can be attributed to the fact that the assumed geometry for the kinematic approach is slightly different for both methods. Thus, the size contacts for both methods are slightly different. In fact, it is shown that under hydrostatic compaction of the unit cell, the contact radius a increases more than the contact width b with increasing relative density for the finite element method. Whereas in the kinematic approach, we have taken a exactly equal to b to obtain the case of hydrostatic compaction.

4 FINITE ELEMENT ANALYSIS

The finite element package ABAQUS[1] is used for the numerical calculations for the the entire compaction process (stages I and II). The representative spherical particle is assumed to be elastic-perfectly plastic solid with a uniaxial yield strength σ_y = 200 MPa, Young's modulus E = 200 GPa and a Poisson's ratio ν=0.3. Regarding the symmetry of the problem only one quarter of the unit cell is considered. The used mesh consists of 1024 quadratic and 176 triangular axisymmetric elements, (*CAX4R*) and (*CAX3*), respectively. All elements are of the hybrid type to permit the modelling of incompressible behaviour.

The deformation of the quarter of the circular cylinder is simulated using two rigid flat punches indenting the grain. Uniform radial u_r and axial u_z displacements are applied incrementally to both frictionless punches. The boundary conditions consist of a zero normal displacement and a zero shear traction along the bottom surface ($z = 0$), a zero radial displacement along the axis of symmetry ($r = 0$) and a free traction at the curved surface of the particle. Different loading paths are achieved by giving different ratios of the displacements u_r and u_z. The macroscopic yield surfaces for isostatic and closed die precompacts at relative density D=0.7, 0.75, 0.8, 0.85, 0.9 and 0.95 are shown in (Σ_r, Σ_z) and (Σ_m, Σ) spaces in *Fig.5,6*. The isostatic precompact has a lower yield stress in uniaxial compression and a higher yield stress in pure radial compression than the closed die precompact, in spite of the fact that both have the same relative density. This implies that the yield behaviour of the spherical particle is not just a function of the relative density but also depends on the previous loading path. Consequently, the macroscopic behaviour of the assembly of the spherical particles is dependent upon the loading history. The shape and size of the the yield surfaces, for both isostatic and closed die precompacts, change as the compaction process passes from stage I densification (D=0.7) to moderate densification (D=0.8) and then to stage II compaction (D=0.95). At all densities, a corner exists at the loading point corresponding to the initial compaction loading path, i.e., the loading path used to

[1] ABAQUS, HKS Inc,Rhode Island, U.S.A.

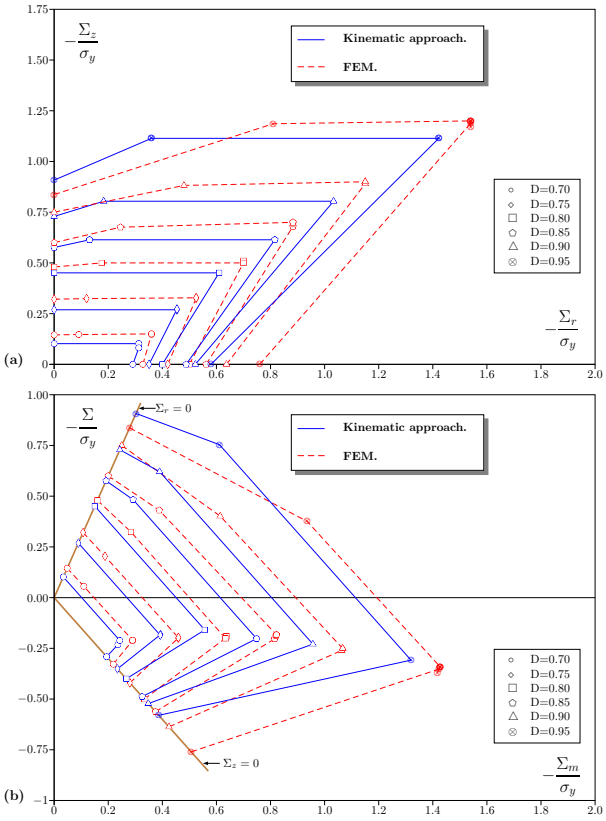

FIG. 5 – Yield surfaces at different relative density values. Comparison of our results to those provided by the FE simulations. Isostatic precompact.

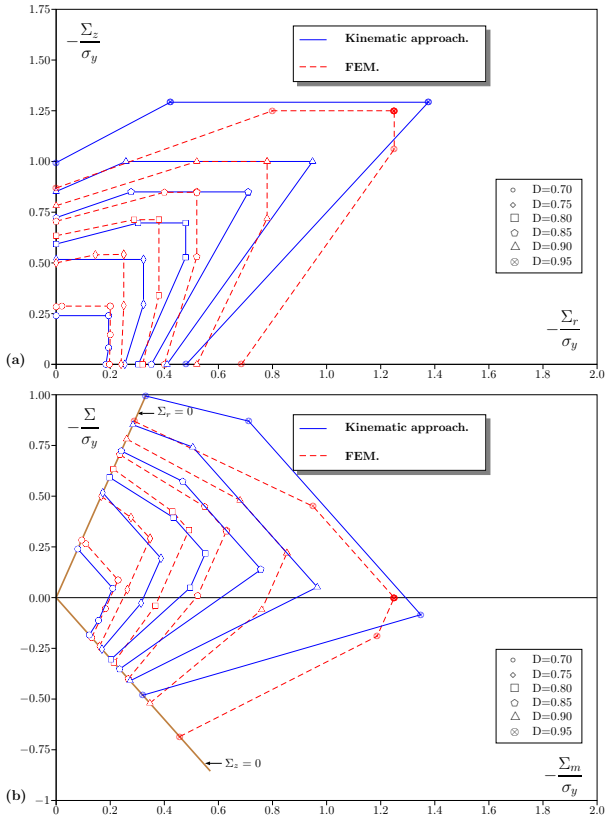

FIG. 6 – Yield surfaces at different relative density values. Comparison of our results to those provided by the FE simulations. Closed die precompact.

produce the precompact.

5 CONCLUDING REMARKS

An analysis based on the kinematic approach of the yields design theory is employed to study the yield surfaces evolution, under hydrostatic and closed die compaction, of a cubic array of spherical particles. In this context, the proposed simple failure mechanisms of an isolated unit cell result in the construction of macroscopic yield surfaces which compare well with the numerical results obtained through the finite element analysis adapted to the problem under consideration. As expected the shape and size of the yield surfaces are found to depend upon the loading history and the relative density of the compacts.

References

[1] SRIDHAR I., FLECK N. A., and AKISANYA A. R. ,"Cold compaction of an array of cylindrical fibres". *Int. J. Mech. Sci.*, 43:715–742, 2001.

[2] SALENÇON J. ,"*Yield design: a survey of the theory*", chapter in Sacchi G. and Salençon J. (eds.), pages 1–44. CISM Lectures, 1993.

[3] OGBONNA N. and FLECK N. A. ,"Compaction of an array of spherical particles". *Acta Metall. Mater.*, 43(2):603–20, 1995.

[4] AKISANYA A. R., COCKS A.C.F., and FLECK N. A. ,"Hydrostatic compaction of cylindrical particles". *J. Mech. Phys. Solids*, 42(7):1067–85, 1994.

[5] HELLE A. S., EASTERLING K. E., and ASHBY M. F. ,"Hot isostatic pressing diagrams: new developments". *Acta metall.*, 33(12):2163–2174, 1985.